

This discussion paper is/has been under review for the journal Biogeosciences (BG).
Please refer to the corresponding final paper in BG if available.

**Regional carbon
fluxes from airborne
flight-path
segmentation**

O. S. Vellinga et al.

Regional carbon dioxide and energy fluxes from airborne observations using flight-path segmentation based on landscape characteristics

O. S. Vellinga^{1,2}, R. W. A. Hutjes², J. A. Elbers², A. A. M. Holtslag¹, and P. Kabat²

¹Wageningen University, Meteorology & Air-Quality Group, Wageningen, The Netherlands

²Wageningen University, Earth-System Science & Climate-Change Group,
Wageningen, The Netherlands

Received: 1 October 2009 – Accepted: 28 October 2009 – Published: 11 November 2009

Correspondence to: O. S. Vellinga (olaf.vellinga@wur.nl)

Published by Copernicus Publications on behalf of the European Geosciences Union.

Title Page

Abstract

Introduction

Conclusions

References

Tables

Figures

⏪

⏩

◀

▶

Back

Close

Full Screen / Esc

Printer-friendly Version

Interactive Discussion

Abstract

This paper presents an analysis of regional fluxes obtained with a small aircraft over heterogeneous terrain in the South West of France, during the large scale field experiment CERES'07. We use a method combining variable flight-path segmentation with basic airborne footprint analysis. The segmentation is based on topography, land use and soil type, using a.o. satellite imagery and digital maps. The segments are delineated using an average footprint length, based on all flights, and segment lengths, which are variable in space but not in time. The method results in segment averaged carbon and energy fluxes, which are shown to be representative of regional fluxes. Our analysis is focussed on the carbon dioxide, heat and evaporative fluxes around solar noon. We will show that spatial and seasonal variations in the fluxes can be linked to the underlying landscape. In addition, a comparison between the airborne data and ground flux data is made to support our results. However, due to the incompleteness of ground data for some predominant vegetation types (even in such a data dense context), upscaling of ground data to regional fluxes was not possible. Without the comparison, we are still able to demonstrate that aircraft can provide direct and meaningful estimates of regional fluxes of energy and carbon dioxide.

1 Introduction

Global atmospheric transport models are used with inverse methods to quantify the carbon balance from atmospheric observations. Powerful at global to continental scale, observational density and methodological progress have lead to useful higher resolution applications (Peters et al., 2007). At the other end of the scale, in the past decades the flux community (e.g. Ameriflux and CarboEurope-IP) has built up extensive networks of flux sites around the world. These networks have been the main source for understanding the local scale processes of the carbon cycle, and process-based models, often in combination with statistical and/or GIS methods to scale up to regional

BGD

6, 10479–10517, 2009

Regional carbon fluxes from airborne flight-path segmentation

O. S. Vellinga et al.

Title Page

Abstract

Introduction

Conclusions

References

Tables

Figures

◀

▶

◀

▶

Back

Close

Full Screen / Esc

Printer-friendly Version

Interactive Discussion

and global scale (e.g. Denning et al., 1999). However, aggregation of processes from bottom-up to larger scales also has its limitations, due to the still low density of flux networks in comparison to the heterogeneity found in the field. The regional scale has been considered as the missing scale between these global and local approaches respectively. Regional budgets and processes might be resolved by obtaining flux data at strategic periods during the annual cycle throughout the atmospheric boundary-layer in an area that is large enough to resolve these processes. In this respect, aircrafts are of particular interest, because they can measure an integral regional flux.

In this context, aircrafts have been involved in atmospheric research for decades. Their contribution is especially known from large field experiments as HAPEX-MOBILHY (André et al., 1986), FIFE (Sellers et al., 1988), BOREAS (Hall, 2001), COBRA (Gerbig et al., 2003), LBA-CLAIRE-98 (Andreae et al., 2001) and RECAP (e.g. Hutjes et al., 2003; Schmitgen et al., 2004; Vila-Guerau de Arellano et al., 2004). From these experiments and others, several studies have been published first focussing on data quality (e.g. Gioli et al., 2004; Mahrt, 1998; Mann and Lenschow, 1994) and data analyses over more or less homogeneous terrain (e.g. Desjardins et al., 1992, 1994; Pérez-Landa et al., 2007; Vaccari et al., 2004). In recent years, research has shifted more to the development of methods for use in much more heterogeneous terrain, like for example sophisticated approaches of flux disaggregation of airborne data obtained over heterogeneous terrain (e.g. Kirby et al., 2008; Ogunjemiyo et al., 2003; Hutjes et al., 2009). Our study presents a basic analysis strategy for regional fluxes using airborne data obtained over heterogeneous terrain during a large field experiment carried out in 2007.

The field experiment during which our data were obtained was the CarboEurope Regional Experiment Strategy (CERES'07, Dolman et al., 2009) as part of the European 6th framework integrated project CarboEurope (<http://www.carboeurope.org/>). It was similar in set-up as the previous campaign, CERES'05, where flux towers, tall towers, radiosondes, and aircrafts were involved to quantify the carbon balance at regional scale in South West France. The experiment *“planned to combine various types of*

BGD

6, 10479–10517, 2009

Regional carbon fluxes from airborne flight-path segmentation

O. S. Vellinga et al.

Title Page

Abstract

Introduction

Conclusions

References

Tables

Figures

⏪

⏩

◀

▶

Back

Close

Full Screen / Esc

Printer-friendly Version

Interactive Discussion

ground-based carbon-cycle related measurements and atmospheric observations with remote sensing to infer a regional carbon budget” (Dolman et al., 2006). CERES’05 ran for a period of six weeks during the growing season in May and June. CERES’07 was completed in two, seasonally complementary campaigns in April (intensive observation period; IOP 1; day 108–112) and September (IOP 2; day 250–258). We have participated in this experiment with our environmental research aircraft (ERA).

In this paper, we present airborne regional carbon and energy fluxes obtained with our ERA during CERES’07. We use a method of variable flight-path segmentation aiming at minimal within segment variability, while linking between segment variation to landscape-scale variations. Our focus will be on the segment averaged turbulent fluxes of carbon-dioxide, heat and water vapour. In addition, a comparison at the regional scale between the airborne data and ground flux data is made to support the results.

2 Experimental set-up

2.1 Area description

Figure 1 shows the experimental domain of CERES’07 (outer box). The area under investigation (150 km × 250 km) is located in the South West of France. It stretches from the city of Toulouse in the East to the Atlantic coast in the West, and from the city of Bordeaux in the North to the Pyrenees mountains in the South. The domain can be divided into four main regions of land use. Along the whole Atlantic coastline between the Pyrenees and Bordeaux, the “Les Landes” forest area stretches halfway inland into the domain in a triangular shape. To the South East of Les Landes towards the Pyrenees, mainly summer crops (sunflowers, maize and vegetables) are grown in complex cultivation patterns. To the North East of Les Landes along the river “Garonne”, vineyards are the main land-use. The Garonne River is the largest river running through the domain between Bordeaux and Toulouse. The remaining part to the East is used for mainly growing winter crops (winter wheat).

BGD

6, 10479–10517, 2009

Regional carbon fluxes from airborne flight-path segmentation

O. S. Vellinga et al.

Title Page

Abstract

Introduction

Conclusions

References

Tables

Figures

⏪

⏩

◀

▶

Back

Close

Full Screen / Esc

Printer-friendly Version

Interactive Discussion

Our flight domain covered the eastern part of the larger CERES'07 experimental area (see inner box Fig. 1). The terrain between the towns of Marmande (MA), Villeneuve-Sur-Lot (hereafter called Villeneuve) and Lamasqu  r   (LA) can be divided into three main regions (see Fig. 2): the river "Garonne" and its valley, the hills to the North East and the geologically different hills to the South West. The main land-use classes (see Sect. 4 for info on land-use map) in the flight domain are "Winter Crops" (WC), "Wheat/Maize" (WM), "Market Gardening" (MG), "Complex Cultivation Patterns with mainly Winter Crops" (CCP/WC), "Complex Cultivation Patterns with mainly Summer Crops" (CCP/SC) and "Mixed Forest" (FO) (see upper plot Fig. 4). Market gardening consists of small scale production of fruits, vegetables, flowers and cash crops, including greenhouses, for the consumer market. Classes CCP/WC and CCP/SC are more specific classes of the original CORINE 2000 class "complex cultivation patterns". Both classes are composed of small parcels of diverse annual crops, pasture and/or permanent crops with one predominant land-use type (SC or WC). In addition, small parcels of arable land, orchards, and city gardens are included in this category. Classes of artificial surfaces (e.g. infrastructure, airports, and urban areas) account for about 4% in this area. The predominant soil types are loam and clay, where clay largely is found in the hills, in some cases mixed with loam. Figure 3 shows the terrain elevation along the flight track between Marmande and Lamasqu  r   with main soil types. The figure shows that the flight track crosses the Garonne Valley three times at different locations, while crossing the river two times.

2.2 Synoptic weather conditions

Both intensive observation periods in April and September were dominated by clear skies with high average maximum daytime temperatures ($\sim 23^{\circ}\text{C}$) and light, variable winds ($\sim 2\text{ m/s}$) with no precipitation. However, two weeks before the start of IOP 1, about 27 mm of precipitation was observed at the ground sites in the area with an average maximum daytime temperature of about 14°C , while in the same period before the start of IOP 2, only about 4 mm of rain with an average maximum daytime temperature

BGD

6, 10479–10517, 2009

Regional carbon fluxes from airborne flight-path segmentation

O. S. Vellinga et al.

Title Page

Abstract

Introduction

Conclusions

References

Tables

Figures

⏪

⏩

◀

▶

Back

Close

Full Screen / Esc

Printer-friendly Version

Interactive Discussion



of about 22°C was observed.

At the start of IOP 1, a high-pressure system (>1025 hPa) was located above western Europe with its center above South West Ireland and a low-pressure system (<1005 hPa) centred above Algeria, Northern Africa. Both systems were moving eastward, gradually weakening somewhat. By the end of the period, their centres were located above the Ukraine (high) and Egypt (low). Between these two larger systems, small highs and lows were developing and disappearing. Meanwhile, a new large high-pressure system was coming in from the Azores. This one developed together with the old high above Ukraine into a blockage over the whole of Europe against a newly developed large low to the West of Ireland.

The second IOP, was dominated by a stationary large high-pressure system (>1030 hPa) above western Europe again with its center above South West Ireland. During the second half of this period, a low pressure-system (<1015 hPa) was moving in from northern Africa. During the IOP, a new high developed above the Azores. By the end of IOP 2, the low was strong enough to divide the high into two regions with one large high above the Atlantic to the west of Portugal and some small highs above central and eastern Europe. The low was now stretching out over most part of France with its center above the coastline of Algeria.

2.3 Instrumentation

Eight ground measurement sites, two tall towers, two radiosonde sites, and five aircraft were involved in the field experiment. Two of the aircraft were almost identical: one operated by the Institute of Biometeorology of the Italian National Research Council (CNR-IBIMET, Italy) and our own. The aircraft is a Sky Arrow 650 ERA with a Mobile Flux Platform (MFP) installed, which was built by Iniziative Industriali Italiane S.p.A. (Rome, Italy) in collaboration with Terrasystem s.r.l. (Viterbo, Italy). The MFP is a collection of instruments built around the Best Atmospheric Turbulence (BAT) probe, developed by the National Oceanic and Atmospheric Administration (NOAA, USA), in conjunction with Airborne Research Australia (ARA, Hacker and Crawford,

Regional carbon fluxes from airborne flight-path segmentation

O. S. Vellinga et al.

Title Page

Abstract

Introduction

Conclusions

References

Tables

Figures



Back

Close

Full Screen / Esc

Printer-friendly Version

Interactive Discussion



1999). Our MFP-system differs from the Italian aircraft (see Gioli et al., 2006, for their type of instruments) only in the temperature probe (by Terrasystem s.r.l.), the GPS/INS (C-Migits™ III by Systron Donner), the net radiation instrument (NR Lite by Kipp & Zonen) and the absence of a dew-point temperature probe. The system is a proven design for airborne measurements of fluxes of carbon dioxide, momentum and heat (Dumas et al., 2001; Gioli et al., 2004). Of the eight ground sites, five were located close to our flight track as shown in Fig. 2: station “Marmande” (MA; 44° 28′ N, 00° 12′ E) maintained by Alterra; stations ‘Saint Sardos’ (SS; 43° 54′ N, 01° 07′ E) and “Le Fauga” (LF; 43° 23′ N, 01° 18′ E) ran by Centre National de Recherches Meteorologiques (CNRM, France); and stations “Auradé” (AU; 43° 33′ N, 01° 07′ E) and “Lamasquère” (LA; 43° 30′ N, 01° 14′ E) operated by Centre d’Etudes Spatiales de la BIOSphère (CESBIO, France).

3 Flight tracks

During IOP 1, we started our flights from the airport of Villeneuve (see Fig. 1). It is located in the middle between Bordeaux to the North West (110 km) and Toulouse to the South East (106 km). In consultation with the team of CNR-IBIMET, we were to cover the South Eastern part of the domain and the Italian team the North Western part. During IOP 2, the airborne headquarters were at the airport of Marmande. This town is located almost in the middle between the Atlantic coastline to the West (115 km) and Toulouse in the South East (140 km). As in IOP 1, we covered the Eastern part of the domain, and the Italian team the Western part. Given the different starting airports, the flight tracks in both IOPs were largely the same, except for the first part. The flight tracks were planned in such a manner that the aircraft flew directly over the ground sites with the intention to validate the airborne data. Several restricted airspaces in the flight domain additionally determined the shape of our flight tracks. Table 1 summarizes the different transect flights carried out during CERES’07. Figure 1 shows the flight domain (inner box) where all our flights were implemented.

Regional carbon fluxes from airborne flight-path segmentation

O. S. Vellinga et al.

Title Page

Abstract

Introduction

Conclusions

References

Tables

Figures



Back

Close

Full Screen / Esc

Printer-friendly Version

Interactive Discussion



During IOP 1, four short (84 km) and five long (173 km) return flights were carried out. In other words, the aircraft made, respectively, eight and ten passes along the flight tracks. The long transect flights covered the full area between Villeneuve and Lamasquère (LA), the short flights only half the distance till Fronton (see Fig. 2). Flights were performed at low air speeds (≈ 37 m/s) to maximize the spatial resolution of our raw data. We flew at low altitude above ground level (≈ 85 m agl, see also Fig. 3), in order to minimize the footprint of our measurements and also to stay well below the “blending height” (Claussen, 1990). From vertical profiles carried out during each transect flight, the boundary-layer depth was determined at around 1.0–1.5 km for all flights. This is supported by radiosonde observations in the area (Sarrat et al., 2009). The flight level is, therefore, within the surface layer for all the flights evaluated in this study. As such, the observed fluxes are expected to be close to the surface fluxes. Similar flights (8 passes; 218 km) were carried out during IOP 2, only now starting at Marmande.

4 Method

To process the raw data, we developed a MATLAB® toolbox with which the three main processing steps can be performed. The toolbox is mainly based on the Unix program MakePOD (Eckman et al., 1999) developed by the NOAA Air Resources Laboratory (ARL-NOAA, USA) and additional code written by B. Gioli of CNR-IBIMET. In the first processing step, data is de-spiked and gap-filled. The data from our MFP hardly contain any spikes due to stable electronics and good weather conditions during both IOPs (see Sect. 2.2). Only the (thin-wire thermocouple-based) temperature signal was occasionally distorted by radio communication between the pilot and air-traffic control. The distorted parts were removed and gap-filled by linear interpolation. In the second processing step, 3D aircraft movements are mathematically compensated for and the signals of the pressure anemometer are converted to wind direction and wind speed. This procedure is specific to our MFP instrumental set-up and airframe configuration.

BGD

6, 10479–10517, 2009

Regional carbon fluxes from airborne flight-path segmentation

O. S. Vellinga et al.

Title Page

Abstract

Introduction

Conclusions

References

Tables

Figures

⏪

⏩

◀

▶

Back

Close

Full Screen / Esc

Printer-friendly Version

Interactive Discussion

In the final processing steps, data are cross-correlated and spatially averaged and fluxes are calculated.

Contrary to tower measurements, fluxes based on aircraft measurements are spatially averaged instead of averaged over time (Crawford et al., 1993). The results hereafter are based on an averaging length of 2000 m, which is at the lower range (2000–4500 m) that has been used before for heterogeneous surfaces (e.g. Desjardins et al., 1994; Ogunjemiyo et al., 2003; Gioli et al., 2004). The processing includes a stationarity test on each averaging window. The window is split in half and the average covariance of each window half $covar(w, F_h)$ needs to be between 0.3–1.7 of the whole averaging window, $covar(w, \overline{F})$, where F can be any flux parameter and subscript h is the index of a window half. Finally, outliers in the flux data were removed using a physical range filter of -250 to 800 W/m^2 for sensible heat (H) and latent heat (λE) flux, and -50 to $50 \mu\text{mol/m}^2/\text{s}$ for carbon-dioxide fluxes (fCO_2). If H and/or λE was discarded, then fCO_2 was discarded as well. We assume that flux divergence was not significant given the combination of boundary-layer heights and flying altitudes for the time periods studied here (between 1200–1400 ST, see below). Therefore, we did not attempt to correct for possible flux divergence.

To derive regional fluxes, we have divided our flight tracks from both IOPs into identical segments with distinct landscape characteristics. Flight-path segmentation is based on geomorphic, soil and vegetation characteristics, using satellite imagery (a.o. Google Earth), a high-resolution elevation map (Farr et al., 2007), a 1-km resolution soil map with USDA texture classification (Fischer et al., 2008), and an enhanced 250-m resolution CORINE 2000 land-use map with 61 classes (Champeaux et al., 2005). Simple footprint-length calculations with the numerical model by Hsieh et al. (2000) served as a tool to determine the upwind distance along which 90 % of the surface flux originated from and thus to identify the predominant land-use classes that govern the fluxes in the segments. For determining an average footprint-length, a roughness length (0.35 m) was chosen to represent the average summed roughness of the vegetation and its terrain in the flight domain. The calculations show that the footprint extends between 3

BGD

6, 10479–10517, 2009

Regional carbon fluxes from airborne flight-path segmentation

O. S. Vellinga et al.

Title Page

Abstract

Introduction

Conclusions

References

Tables

Figures

⏪

⏩

◀

▶

Back

Close

Full Screen / Esc

Printer-friendly Version

Interactive Discussion

and 6 km upwind of the flight track. Neglecting wind direction (because wind speeds generally were very low), the average footprint length determined the width on both sides along the flight track to extract data from the land-use map. These what we call “segment areas” should be a good indication of the area, influencing our segment fluxes as we will see in Sect. 6.

Figure 4 shows that our flight tracks well represent the whole square study domain, as the distribution of land-use classes for the extracted part along the flight path (lower plot) is very similar to the one for the whole flight domain (upper plot). As shown in the lower plot, the exact footprint length (3 or 6 km) does not have a significant effect on the land-cover distribution. In this study, we use the more conservative footprint-length estimate of 3 km. Largest differences between segment areas and full domain are found in classes MG (23%), WM (11%), and WC (16%). However, together with classes CCP/WC (15%) and CCP/SC (10%), these land-use classes dominate both the domain and the segment areas. MG and WM are found in the river valley, and CCP, SC and WC in the hills. In some areas along the flight track, other land-use classes dominate, which are pastures (PA), fruit/berry plantations (FB), bordelais vineyards (VY) and mixed forest (FO; not the official CORINE class), and consequently, these were put in their own segments. This resulted in 12 segments with varying lengths (on average 19 km) as shown in Fig. 2 and 3, and as described in Table 2.

After dividing the flight tracks into segments, measured data belonging to a particular segment was averaged for each flight passes as in formula 1:

$$\bar{F}_{i,j} = \frac{\sum_{k=1}^n F_{i,j,k}}{n_{i,j}} \quad (1)$$

where $\bar{F}_{i,j}$ = average flux per flight pass (j) per segment (i); $F_{i,j,k}$ = 2-km flux (k) per flight pass per segment; and $n_{i,j}$ = number of 2-km fluxes per flight pass per segment. This results in one average flux (e.g. one carbon-dioxide flux) for each segment per flight pass.

Regional carbon fluxes from airborne flight-path segmentation

O. S. Vellinga et al.

Title Page

Abstract

Introduction

Conclusions

References

Tables

Figures

⏪

⏩

◀

▶

Back

Close

Full Screen / Esc

Printer-friendly Version

Interactive Discussion

Finally, all averaged data per segment have been once more averaged for all flight passes per IOP according to formula 2:

$$\bar{F}_i = \frac{\sum_{j=1}^m \bar{F}_{i,j}}{m_i} \quad (2)$$

where \bar{F}_i = averaged flux per segment (i); $\bar{F}_{i,j}$ = averaged flux per flight pass (j) per segment (i) resulting from formula 1; and m_i = number of flight passes per segment. This results in one average flux for each segment per IOP.

To prevent the influence of variations on these averages, caused by the diurnal cycle (due to varying time of overflight at each location), we only selected flight data between 1200 and 1400 local solar time (i.e. UTC = LT - 2). This implied that five outward flights between Villeneuve and Lamasquère were selected from IOP 1, and four return flights between Lamasquère and Marmande from IOP 2. Thus, for IOP 1, the time of day progresses from segment 1 to the last segment, while for IOP 2, it is the opposite starting at segment 12 and ending at segment 1. Due to this narrow time filter, no segment averages are available for segment 1 and 2 in IOP 1, and for segments 1 to 3 in IOP 2.

To further reduce the effect of diurnal variability we analysed heat fluxes indirectly as ratio's, since both the evaporative fraction ($E_f = \lambda E / (\lambda E + H)$) and the Bowen ratio ($\beta = H / \lambda E$) are generally more conservative in time than the absolute magnitude of the fluxes.

5 Results

Table 2 describes the different segments presenting only those land-use classes that take up more than 10% of the segment area. The table shows that class MG is the dominant land use in the area (segments 1, 5–9 and 12). Second most common land use in the area is class CCP/WC found in segments 1, 4–9 and 12, of which segment 4

Regional carbon fluxes from airborne flight-path segmentation

O. S. Vellinga et al.

Title Page

Abstract

Introduction

Conclusions

References

Tables

Figures

⏪

⏩

◀

▶

Back

Close

Full Screen / Esc

Printer-friendly Version

Interactive Discussion



is the only segment with predominant class CCP/WC. The latter additionally has the largest land-use fractions for class “Agricultural Clusters”. However, segments 10 and 11 have virtually only fields with winter crops. Segments 9 and 12 are rather similar in composition and have class WM as their third largest land use. Class “Wheat/Maize” is also a large part of segments 2–4 and 6. Segments 2 and 3 have the same three largest land-use types (CCP/SC, WM and PA), only in different order. Segment 2 is the only segment with the predominant class CCP/SC, while for segment 3, this is class WM. They both are the only two segments with the largest fraction of class PA. Segment 7 consist for about half the area of class ‘Bordelais Vineyards’ (VY). Furthermore, large fractions of CCP/SC can be found in segments 2–4 and 6. In addition, segment 6 has the highest number of classes, including the only one with class FO. Finally, class “Fruit/Berry Plantations” (FB) and class “Broad Leaf Trees + Crops” are only found in, respectively, segment 5 and 8.

For the same segment areas, we retrieved an average leaf area index (LAI) from MODIS data of the Terra (EOS AM) satellite. Figure 5 shows the average LAI per segment for 15–22 April 2007 and for 6–13 September 2007. These time windows overlap with respectively IOP 1 and IOP 2. First, notice the clear difference in magnitude of LAI for both IOPs; April shows larger values than September when many crops were either harvested (winter wheat) or ripening and largely senescent (e.g. sun flowers). Secondly, during IOP 1, the LAI roughly increases from segment 1 to the last segment, starting at about 1.0 in the first segments and ending at about 1.5 in the last segments. During IOP 2, it is more or less the opposite, values of about 1.25 in the first segments down to about 0.7 in the last ones. These spatial patterns reflect the dominance of winter crops in higher numbered segments and that of late crops (e.g. maize) in the first few segments.

Net radiation (Q^*) and incoming photosynthetically active radiation (PAR_i) in the clear sky conditions of our IOPs merely exhibit temporal – but no significant spatial – variations. Therefore, they are good indicators for the performance of our time filter. The average net radiation per segment for IOP 1 and IOP 2 are presented in Table 3 and

BGD

6, 10479–10517, 2009

**Regional carbon
fluxes from airborne
flight-path
segmentation**

O. S. Vellinga et al.

Title Page

Abstract

Introduction

Conclusions

References

Tables

Figures

⏪

⏩

◀

▶

Back

Close

Full Screen / Esc

Printer-friendly Version

Interactive Discussion

4, respectively. During IOP 1, the net radiation stays constant at about 560 W/m^2 between segments 3 and 6 and afterwards decreases somewhat gradually to about 490 W/m^2 in the last segment. During IOP 2, the net radiation is on average lower and has larger error bars (not presented here) than during IOP 1. It increases between segment 4 to 10 from about 430 W/m^2 to about 490 W/m^2 , and stays after that at about 450 W/m^2 . The PAR_i (not shown here) shows for both periods somewhat the same, but less pronounced trend and change in error bars. During IOP 1, PAR_i decreases from about $1700 \mu\text{E/m}^2$ to about $1400 \mu\text{E/m}^2$, while during IOP 2, it stays somewhat constant at about $1400 \mu\text{E/m}^2$. Both radiation parameters show some residual diurnal influence, opposite between both IOPs, caused by the selected outward flights for IOP 1 and return flights for IOP 2. We may conclude that the time filter worked well: light conditions were nearly identical during all flights ($CV < 10\%$), though minor temporal trends still can be taken into account, when interpreting the segment averaged fluxes.

Figures 6 and 7 show for IOP 1 (April) and IOP 2 (September), the segment averages of, respectively, the Bowen ratio ($[\bar{\beta}]_{\text{seg}}$) and the evaporative fraction ($[\bar{E}_f]_{\text{seg}}$). They show that $[\bar{\beta}]_{\text{seg}}$ is much lower during IOP 1 compared to IOP 2. For $[\bar{E}_f]_{\text{seg}}$, it is then the opposite, where IOP 2 is about 20% lower than IOP 1. This corresponds with ground observations along the flight track as can be seen in Table 5. In addition, the results correspond with the amount of precipitation in the periods before the start of both IOPs, mentioned in Sect. 2.2. As these two ratios can be considered to be rather independent from the diurnal cycle, the variations in these fractions within each IOP are mostly related to the underlying landscape, while the differences between IOPs can be related to seasonal change.

Figure 8 and 9 show the average carbon-dioxide flux per segment ($[\overline{fCO_2}]_{\text{seg}}$), respectively for IOP 1 and IOP 2. The figures show that there was more carbon uptake during IOP 1 than during IOP 2, except for segment 6 and 7. This corresponds with the higher LAI and evaporative fractions found for IOP 1 as photosynthesis is coupled

**Regional carbon
fluxes from airborne
flight-path
segmentation**

O. S. Vellinga et al.

Title Page

Abstract

Introduction

Conclusions

References

Tables

Figures

⏪

⏩

◀

▶

Back

Close

Full Screen / Esc

Printer-friendly Version

Interactive Discussion

to plant transpiration and both are also a function of leaf area. The correlation is, however, not strong, because latent heat flux includes evaporation from soil and water bodies as well and likewise the carbon flux includes soil respiration. The larger carbon uptake during IOP 1 compared to IOP 2 is consistent with the seasonal variation in crops as explained above for LAI. Looking at the differences between segments within each IOP, the carbon dioxide flux for IOP 1 shows marked differences compared to IOP 2. During IOP 1, the carbon uptake decreases between segments 3 to 6 from about $-11 \mu\text{mol}/\text{m}^2/\text{s}$ to about zero flux and afterwards increases again to more than $-10 \mu\text{mol}/\text{m}^2/\text{s}$ in segments 10 and 11, followed by a decrease in the last segment to about $-6 \mu\text{mol}/\text{m}^2/\text{s}$. As for IOP 2, the carbon uptake increases between segments 4 and 6 from about $-3 \mu\text{mol}/\text{m}^2/\text{s}$ to about $-7 \mu\text{mol}/\text{m}^2/\text{s}$, then decreases again in segment 11 to about $-1 \mu\text{mol}/\text{m}^2/\text{s}$ with peak values in segments 8 and 12 of about $-7 \mu\text{mol}/\text{m}^2/\text{s}$ and $-5 \mu\text{mol}/\text{m}^2/\text{s}$, respectively.

The fluxes of some segments can be clearly related to their dominant land-use classes. First, segments 4, 10 and 11 contain winter crops (WC). In April, winter crops were fully developed in this area, while in September, the same fields were bare. This is clearly represented by ground site "Lamasqu  r  " (LA), where during IOP 1, LA shows a high LAI, a large carbon uptake and a high evaporation, whereas during IOP 2 there was practically no carbon flux or evaporation from the then bare field (see Table 5). A similar change can be found in our airborne carbon uptake ($[\overline{fCO_2}]_{\text{seg}}$) of segments 4, 10 and 11 in Table 3 and 4. However, the change is more profound for segments 10 and 11, because their areas consist for more than 80 % of winter crops. Segment 4 is a complex, largely unknown mixture of land use, of which only part is winter crops in CCP/WC (see Table 2). This means that other types of land use within the segment may have resulted in the still significant carbon uptake in IOP 2. For example, class WM and class CCP/SC are fully matured in September which is shown for maize at station 'Marmande' (MA) in Table 5. The leaf area index for those segments supports this change between both periods (see Table 3 and 4). Here, segments 10 and 11 have a larger decrease in LAI than segment 4. Less obvious are the changes for E_f and β

Regional carbon fluxes from airborne flight-path segmentation

O. S. Vellinga et al.

Title Page

Abstract

Introduction

Conclusions

References

Tables

Figures

⏪

⏩

◀

▶

Back

Close

Full Screen / Esc

Printer-friendly Version

Interactive Discussion

between the segments for both IOPs, although they agree with changes in LAI. The latter means bare fields in dry periods have a large β and a small E_f . Bare soils lose their soil humidity in the top layer much quicker than when covered with vegetation, because on bare soils, water evaporates and runs through the soil more quickly. In the end, this results in a smaller λE and a larger H as there is almost no water to evaporate.

Secondly, segment 7 has almost 50% vineyards and shows more carbon uptake in IOP 2 than in IOP 1. This can be explained by the growth stage of the vineyards and class "Market Gardening". In April, these vineyards are still building up their leaves and grapes, whereas in September, they are fully matured. Measurements by CNRM at vineyard station "Fronton" (see Fig. 2) during the previous campaign (CERES'05) show that the LAI increases from 0.3 in April to 1.4 in mid-August. The LAI of the vineyards stays low due to their low soil coverage. However, our segment averaged LAI, found here via MODIS data (see Table 3 and 4), decreases from about 1.2 to 0.9. This decrease can be explained by the presence of class CCP/WC which includes winter crops that are absent during September. The end result is a modest increase in carbon uptake. Class MG might have supported this increase. The early growth stage of vineyards in April and the complex structure of the remaining part of segment 7 has probably influenced the variability in the data (i.e. large error bars), during IOP 1, compared to IOP 2.

More complex are all remaining segments with class MG as the predominant land-use class, which accounts for more than 30% in each segment area. Segment 5, 6, 8, 9 and 12 have on average 41% of MG in their segment area. All of these segments, except for segment 6, show less carbon uptake during IOP 2 than during IOP 1. When trying to relate the fraction of MG to the changes of carbon uptake within each segment no clear correlation appears. This is probably due to highly mixed and heterogeneous character of this land-use class. Class MG contains small scale winter and summer crops, but both can vary from segments to segment. Other land-use fractions and other factors may play a role in these segments (see Table 2).

Segment 9 and 12 have similar compositions of major land-use fractions (i.e. MG,

**Regional carbon
fluxes from airborne
flight-path
segmentation**O. S. Vellinga et al.

[Title Page](#)[Abstract](#)[Introduction](#)[Conclusions](#)[References](#)[Tables](#)[Figures](#)[⏪](#)[⏩](#)[◀](#)[▶](#)[Back](#)[Close](#)[Full Screen / Esc](#)[Printer-friendly Version](#)[Interactive Discussion](#)

CCP/WC and WM). As seen from Table 3 and 4, this results in somewhat the same decrease in carbon uptake for each segment between both IOPs. Still, segment 12 shows a decrease $1.5 \mu\text{mol}/\text{m}^2/\text{s}$, while segment 9 decreases with $0.9 \mu\text{mol}/\text{m}^2/\text{s}$. This difference corresponds with the segment averaged LAI in Table 3 and 4, where the LAI in segment 12 shows a larger decrease than in segment 9. Although, β and E_f correspond with LAI, there is no significant difference between the two segments. Explaining the reduced carbon uptake in segment 12 may be the larger fractions of CCP/WC and WM, but smaller fraction of MG, in the segment. Unfortunately, ground sites “St. Sardos” (SS) in segment 9 and “Le Fauga” (LF) in segment 12 cannot be used as a reference due to the different land use they were installed.

Segment 8 has the largest fraction of class MG, but it is the smallest segment with a length of 5 km and an area of 14 km^2 (see Table 2). In other words, $[\overline{fCO_2}]_8$ is to a larger extend affected by its neighbouring segments compared to the other segment averaged fluxes. As the segments have unequal lengths, the extend of influence of neighbouring segments differs for each segment. In this study, the carbon-dioxide fluxes are based on an averaging length of 2 km, which means that 2–3 length averaged fluxes fall within segment 8 for each flight pass. If, for a flight pass, segment 8 holds only two 2-km fluxes, then those fluxes are calculated from raw data within segment 8. However, if three 2-km fluxes fall within the segment, then one flux has partially been calculated from (maximum 1000 m of) raw data belonging to one of the neighbouring segments. This might be the reason that segment 8 shows the largest error bars during IOP 1. The segment averaged LAI in segment 8 decreases during IOP 2, which suggests that the decrease in carbon uptake between both IOPs is reasonable. In addition, less carbon uptake in segment 8 during IOP 2 can partially be explained by the presence of winter crops through class CCP/WC, but is probably dominated by changes in class MG. The third largest land-use fraction is “Broad Leaf Trees+Crops”, which accounts for 11 %, has probably had a compensating effect on the segment averaged carbon-dioxide flux of segment 8.

Segment 5 is somewhat similar to segment 8 for the three major land-use fractions

Regional carbon fluxes from airborne flight-path segmentation

O. S. Vellinga et al.

Title Page

Abstract

Introduction

Conclusions

References

Tables

Figures

⏪

⏩

◀

▶

Back

Close

Full Screen / Esc

Printer-friendly Version

Interactive Discussion

(see Table 2). However, segment 5 has smaller fractions of class MG (43 %) and class CCP/WC (14 %), and it has “Fruit and Berry Plantations” (FB; 13 %) as the third largest land use instead. The carbon uptake in segment 5 shows a smaller decrease than the one in segment 8. This corresponds with the segment averaged LAI for segment 5, which is smaller and decreases less, than the one for segment 8. In turn, β and E_f correlates with these changes in LAI. Moreover, the carbon uptake in segment 5 shows the smallest change (about $0.9 \mu\text{mol}/\text{m}^2/\text{s}$) between both periods. The decrease can be explained by the winter crops in class CCP/WC. To compensate it, class FB may have had a larger effect than class “Broad Leaf Trees+Crops” in segment 8.

Segment 6 shows the largest increase of carbon uptake of all segments, here (see Table 3 and 4). In addition, it is the most complex segment with regard to the number of large land-use fractions ($>10\%$) as also indicated by the large error bars. During IOP 1, it has the largest β , which corresponds with the observed carbon flux close to zero for this period. During IOP 2, it has the second lowest β , which additionally corresponds with one of the highest carbon uptake during this period. However, for both periods, it has one of the highest LAI and the decrease in LAI is the smallest of all segments. The large LAI with its small decrease and the increase in carbon uptake seem contradictory. Class FO, which includes among others coniferous trees, might be responsible for the large LAI during IOP 1. On the other hand, the same class FO contains broad leaf trees as well. This class, and classes ‘WM’ and ‘CCP/SC’ might explain the large increase in carbon uptake. These classes account together for about 47 % of the segment area, all containing vegetation that is fully matured during the summer season. The decrease in LAI due to the winter crops in other classes, including class FO, might have been compensated by these classes.

6 Discussion

Overall, the airborne flux data seem to be consistent with the underlying terrain and to reflect true seasonal variations. Some methodological points of discussion still remain.

BGD

6, 10479–10517, 2009

Regional carbon fluxes from airborne flight-path segmentation

O. S. Vellinga et al.

Title Page

Abstract

Introduction

Conclusions

References

Tables

Figures

⏪

⏩

◀

▶

Back

Close

Full Screen / Esc

Printer-friendly Version

Interactive Discussion



**Regional carbon
fluxes from airborne
flight-path
segmentation**O. S. Vellinga et al.

[Title Page](#)[Abstract](#)[Introduction](#)[Conclusions](#)[References](#)[Tables](#)[Figures](#)[⏪](#)[⏩](#)[◀](#)[▶](#)[Back](#)[Close](#)[Full Screen / Esc](#)[Printer-friendly Version](#)[Interactive Discussion](#)

so-called “segment areas” based on averaged, first order estimates of footprint length followed by an analysis of the segment area. In our analysis using a double footprint area (6 km on either side of the flight track instead of 3 km) did not significantly change the land-cover class distributions or characteristics like LAI, justifying our choice for the simple and more conservative approach.

Finally, the influence of diurnal variations on segment averages has been minimized by selecting only data obtained between 1200 and 1400 local solar time. However, some small degree of diurnal effect remains as illustrated by the segment averaged Q^* in Table 3 and 4. Within this time window, the flight track during IOP 1 was flown in opposite direction compared to IOP 2. Nevertheless, given that the total coefficient of variation of Q^* is less than 10 %, we believe this effect did not significantly influence our results.

To investigate the extend to which our airborne data compare with the ground data, we need to upscale the ground data to regional scale since a direct comparison between airborne data and ground data is not possible (Mahrt, 1998; Gioli et al., 2004). In principle, the distribution of land-use fractions along the flight tracks (see Fig. 4) can be used together with ground-based flux magnitudes to do this. Table 5 shows that the ground sites provide data for land-use classes SC, WM, WC and “Natural Grasslands Cluster” (NGC), while data on the largest class MG is missing. For classes CCP/SC and CCP/WC, the fraction of SC and WC needs to be estimated. When assuming that 2/3 of classes CCP/SC and CCP/WC is WC and SC, the available ground data covers only about 45 % of the whole area along the flight tracks. In addition, with regard to the used land-use map, Sarrat et al. (2009) found that land-use classes WM and WC are underestimated and overestimated by about 40 %, respectively. This was confirmed by our visual inspections during the flights, which also indicated more maize on the ground than the land-use map suggests. Filling the gap for the missing classes by numerical modelling of fluxes from vegetation would further introduce more complexity to the results. The uncertainties with respect to the land cover in the area, combined with still fragmentary ground data made us refrain from a pure data-based upscaling.

**Regional carbon
fluxes from airborne
flight-path
segmentation**

O. S. Vellinga et al.

Title Page

Abstract

Introduction

Conclusions

References

Tables

Figures



Back

Close

Full Screen / Esc

Printer-friendly Version

Interactive Discussion



7 Conclusions

The main goal of this study is to find a method for retrieving regional fluxes from an airborne data-set of the field experiment CERES'07 for investigating temporal and spatial variations in the fluxes linked to the underlying heterogeneous landscape. Focus has been on the carbon uptake during two IOPs at CERES'07. Our method consists of flight-path segmentation based on homogeneous landscape characteristics. The carbon uptake can be related in a meaningful way to seasonal trends and variations in land use. The land-use distribution of the extracted part along the flight track does not considerably differ from the one of the whole flight domain (see Fig. 4). So, we can get a good idea about the carbon uptake for the whole flight domain (see inner box in Fig. 1) by determining the weighted average carbon uptake of all segments (see Table 2). This shows that the average carbon uptake for IOP 1 (April) is $-7.0 \mu\text{mol}/\text{m}^2/\text{s}$, which is larger than IOP 2 (September) with an average of $-3.7 \mu\text{mol}/\text{m}^2/\text{s}$. The carbon uptake correlates well with the leaf area index from MODIS between the segments and between the IOPs. In particular, the contrast between segments with predominantly winter crops and other segments is clearly visible. The energy fluxes support the seasonal change in carbon uptake and leaf area index, but do not clearly show differences between the segments within an IOP. Again, scaling up the results to the total area of all segments shows an average Bowen ratio of 0.49 in April (IOP 1) or an evaporative fraction of 0.67. In September (IOP 2), these numbers are $\beta = 1.76$ and $E_f = 0.36$. The carbon and energy fluxes, though consistent with data from ground stations, cannot be quantitatively compared, because ground data were incomplete with regard to the land-cover classes covered and because of uncertainties in the land-cover map. Instead, we believe that airborne fluxes averaged and segmented in relation to variability at the landscape scale are in themselves very useful to quantify regional fluxes for energy and carbon dioxide in a direct way. Regional estimates that can be used as a reference for other estimates, whether they are based on inverse methods from, for example, tall tower measurements or model based on, for instance, remote-sensing

BGD

6, 10479–10517, 2009

Regional carbon fluxes from airborne flight-path segmentation

O. S. Vellinga et al.

Title Page

Abstract

Introduction

Conclusions

References

Tables

Figures

⏪

⏩

◀

▶

Back

Close

Full Screen / Esc

Printer-friendly Version

Interactive Discussion

derived vegetation characteristics.

Acknowledgements. This study was jointly supported by the European Framework Programme 6 Integrated Project CarboEurope (GOCE-CT2003-505572), by the Dutch national research programme “Climate changes Spatial Planning” (www.climatechangesspatialplanning.nl), and by the Strategic Knowledge Development Programme of Wageningen UR on Climate Change (Kennisbasis thema Klimaatverandering) funded by the Dutch ministry of Agriculture, Nature and Food Quality. We thank our pilots of the Aero Company Vliegschool Teuge BV (ACVT, Netherlands) for their careful, terrain hugging flight manoeuvres. Many thanks go to Beniamino Gioli and Franco Miglietta at CNR-IBIMET and to Ed Dumas at ARL-NOAA for their highly appreciated support in developing the processing software. For this, a working visit at CNR-IBIMET was funded by the Netherlands Organisation of Scientific Research (NWO). Last but not least, thanks go to all colleagues of the CarboEurope-IP Regional Experiment for the pleasant collaboration during the field campaigns.

References

- André, J., Goutorbe, J., and Perrier, A.: HAPEX—MOBILHY: A hydrologic atmospheric experiment for the study of water-budget and evaporation flux at the climatic scale, *B. Am. Meteor. Soc.*, 67, 138–144, 1986. 10481
- Andreae, M. O., Artaxo, P., Fischer, H., Freitas, S. R., Grégoire, J. M., Hansel, A., Hoor, P., Kormann, R., Krejci, R., Lange, L., Lelieveld, J., Lindinger, W., Longo, K., Peters, W., de Reus, M., Scheeren, B., Silva Dias, M. A. F., Ström, J., van Velthoven, P. F. J., and Williams, J.: Transport of Biomass Burning Smoke to the Upper Troposphere by Deep Convection in the Equatorial Region, *Geophys. Res. Lett.*, 28, 951–954, 2001. 10481
- Champeaux, J.-L., Fortin, H., and Han, K.-S.: Spatio-Temporal Characterization of Biomes over SW of France using SPOT/VEGETATION and CORINE Land Cover Datasets, in: *Geoscience and Remote Sensing Symposium, 2005, IGARSS'05, Proc. 2005 IEEE Int.*, 2, 1295–1298, 2005. 10487
- Claussen, M.: Area-averaging of surface fluxes in a neutrally stratified, horizontally inhomogeneous atmospheric boundary layer, *Atmos. Environ.*, 24 A, 1349–1360, 1990. 10486
- Crawford, T. L., McMillen, R. T., Dobosy, R. J., and MacPherson, I.: Correcting airborne flux measurements for aircraft speed variation, *Bound.-Lay. Meteorol.*, 66, 237–245, 1993. 10487

10499

BGD

6, 10479–10517, 2009

Regional carbon fluxes from airborne flight-path segmentation

O. S. Vellinga et al.

Title Page

Abstract

Introduction

Conclusions

References

Tables

Figures

⏪

⏩

◀

▶

Back

Close

Full Screen / Esc

Printer-friendly Version

Interactive Discussion



**Regional carbon
fluxes from airborne
flight-path
segmentation**O. S. Vellinga et al.

[Title Page](#)[Abstract](#)[Introduction](#)[Conclusions](#)[References](#)[Tables](#)[Figures](#)[⏪](#)[⏩](#)[◀](#)[▶](#)[Back](#)[Close](#)[Full Screen / Esc](#)[Printer-friendly Version](#)[Interactive Discussion](#)

- Denning, A. S., Takahashi, T., and Friedlingstein, P.: Can a strong atmospheric CO₂ rectifier effect be reconciled with a “reasonable” carbon budget?, *Tellus B*, 51, 249–253, 1999. 10481
- Desjardins, R. L., Hart, R. L., Macpherson, J. I., Schuepp, P. H., and Verma, S. B.: Aircraft-Based and Tower-Based Fluxes of Carbon-Dioxide, Latent, and Sensible Heat, *J. Geophys. Res.-Atmos.*, 97, 18477–18485, 1992. 10481
- Desjardins, R. L., MacPherson, J. I., Schuepp, P. H., and Hayhoe, H. N.: Airborne flux measurements of CO₂, sensible, and latent heat over the Hudson Bay lowland, *J. Geophys. Res.*, 99, 1994. 10481, 10487
- Dolman, A. J., Noilhan, J., Durand, P., Sarrat, C., Brut, A., Pignatelli, B., Butet, A., Jarosz, N., Brunet, Y., Loustau, D., Lamaud, E., Tolk, L., Ronda, R., Miglietta, F., Gioli, B., Magliulo, V., Esposito, M., Gerbig, C., Körner, S., Glademard, P., Ramonet, M., Ciais, P., Neininger, B., Hutjes, R. W. A., Elbers, J. A., Macatangay, R., Schrems, O., Pérez-Landa, G., Sanz, M. J., Scholz, Y., Facon, G., Ceschia, E., and Beziat, P.: The CarboEurope Regional Experiment Strategy, *B. Am. Meteor. Soc.*, 87, 1367–1379, 2006. 10482
- Dolman, A. J., Gerbig, C., Noilhan, J., Sarrat, C., and Miglietta, F.: Detecting regional variability in sources and sinks of carbon dioxide: a synthesis, *Biogeosciences*, 6, 1015–1026, 2009, <http://www.biogeosciences.net/6/1015/2009/>. 10481
- Dumas, E., Brooks, S., and Verfaillie, J.: Development and Testing of a Sky Arrow 650 ERA Aircraft for Atmospheric Research, in: 11th Symposium on Meteorological Observations and Instrumentation (14–18 January 2001 Albuquerque, New Mexico) Near Fine, American Meteorological Society’s 81st Annual Meeting, American Meteorological Society, Kluwer Academic Publishers, Dordrecht, The Netherlands, 2001. 10485
- Eckman, R., Crawford, T., Dumas, E., and Birdwell, K.: Airborne Meteorological Measurements Collected During The Model Validation Program (Mvp) Field Experiments At Cape Canaveral, Florida, Technical Memorandum ARL/ATDD-233, NOAA/ARL, Silver Spring (Maryland), USA, 1999. 10486
- Farr, T., Rosen, P., Caro, E., Crippen, R., Duren, R., Hensley, S., Kozubick, M., Paller, M., Rodriguez, E., Roth, L., Seal, D., Shaffer, S., Shimada, J., Umland, J., Werner, M., Oskin, M., Burbank, D., and Alsdorf, D.: The shuttle radar topography mission, *Rev. Geophys.*, 45, 2007. 10487
- Fischer, G., Nachtergaele, F., Prieler, S., van Velthuisen, H., Verelst, L., and Wiberg, D.: Global Agro-ecological Zones Assessment for Agriculture (GAEZ 2008), <http://www.iiasa.ac.at/Research/LUC/luc07/External-World-soil%-database/>, 2008. 10487

- Gerbig, C., Lin, J. C., Wofsy, S. C., Daube, B. C., Andrews, A. E., Stephens, B. B., Bakwin, P. S., and Grainger, C. A.: Toward constraining regional-scale fluxes of CO₂ with atmospheric observations over a continent: 2. Analysis of COBRA data using a receptor-oriented framework, *J. Geophys. Res.-Atmos.*, 108, 1–19, 2003. 10481
- 5 Gioli, B., Miglietta, F., De Martino, B., Hutjes, R. W. A., Dolman, H. A. J., Lindroth, A., Schumacher, M., Sanz, M. J., Manca, G., Peressotti, A., and Dumas, E. J.: Comparison between tower and aircraft-based eddy covariance fluxes in five European regions, *Agr. For. Meteorol.*, 127, 1–16, 2004. 10481, 10485, 10487, 10497
- 10 Gioli, B., Miglietta, F., Vaccari, F. P., Zaldei, A., and De Martino, B.: The Sky Arrow ERA, an innovative airborne platform to monitor mass, momentum and energy exchange of ecosystems, *Ann. Geophys.*, 49, 109–116, 2006, <http://www.ann-geophys.net/49/109/2006/>. 10485
- Hacker, J. M. and Crawford, T. L.: The BAT-Probe: The ultimate tool to measure turbulence from any kind of aircraft (or sailplane), *Tech. Soar.*, 23, 42–45, 1999. 10484
- 15 Hall, F. G.: Introduction to special section: BOREAS III, *J. Geophys. Res.-Atmos.*, 106, 33511–33516, 2001. 10481
- Hsieh, C. I., Katul, G., and Chi, T.: An approximate analytical model for footprint estimation of scalar fluxes in thermally stratified atmospheric flows, *Adv. Water Res.*, 23, 765–772, 2000. 10487
- 20 Hutjes, R., Van den Bulk, W., Cosin, S., Erisman, J., Fritsch, H., Gioli, B., Grelle, A., Hensen, A., Lagergren, F., Lindroth, A., Ter Maat, H., Mantilla, E., Miglietta, F., Millán, M., Mölder, M., Ouden, A. d., Pérez, G., Ronda, R., Sanz, M., Schmitgen, S., Schumacher, M., Tuulik, J., Vermeulen, A., and Vilà-Guerau de Arellano, J.: Regional Assessment and Monitoring of the Carbon Balance within Europe (RECAB), *Tech. Rep. EVK2-CT-1999-00034*, Wageningen UR, Alterra, 2003. 10481
- 25 Hutjes, R., Vellinga, O., Gioli, B., and Miglietta, F.: Dis-aggregation of airborne flux measurements using footprint analysis, *Agr. For. Meteorol.*, submitted, 2009. 10481
- Kirby, S., Dobosy, R., Williamson, D., and Dumas, E.: An aircraft-based data analysis method for discerning individual fluxes in a heterogeneous agricultural landscape, *Agr. For. Meteorol.*, 148, 481–489, 2008. 10481
- 30 LeMone, M. A., Grossman, R. L., Chen, F., Ikeda, K., and Yates, D.: Choosing the Averaging Interval for Comparison of Observed and Modeled Fluxes along Aircraft Transects over a Heterogeneous Surface, *J. Hydrometeorol.*, 4, 179–195, 2003. 10496
- Lyons, T. J., Fuqin, L., Hacker, J. M., Cheng, W.-L., and Xinmei, H.: Regional turbulent statistics

BGD

6, 10479–10517, 2009

**Regional carbon
fluxes from airborne
flight-path
segmentation**

O. S. Vellinga et al.

Title Page

Abstract

Introduction

Conclusions

References

Tables

Figures

◀

▶

◀

▶

Back

Close

Full Screen / Esc

Printer-friendly Version

Interactive Discussion

- over contrasting natural surfaces, *Meteorol. Atmos. Phys.*, 78, 183–194, 2001. 10496
- Mahrt, L.: Flux sampling errors for aircraft and towers, *J. Atmos. Ocean. Technol.*, 15, 416–429, 1998. 10481, 10497
- Mann, J. and Lenschow, D. H.: Errors in airborne flux measurements, *J. Geophys. Res.-Atmos.*, 99, 14519–14526, 1994. 10481
- Ogunjemiyo, S. O., Kaharabata, S. K., Schuepp, P. H., MacPherson, I. J., Desjardins, R. L., and Roberts, D. A.: Methods of estimating CO₂, latent heat and sensible heat fluxes from estimates of land cover fractions in the flux footprint, *Agr. For. Meteorol.*, 117, 125–144, 2003. 10481, 10487
- Pérez-Landa, G., Ciais, P., Sanz, M. J., Gioli, B., Miglietta, F., Palau, J. L., Gangoiti, G., and Millán, M. M.: Mesoscale circulations over complex terrain in the Valencia coastal region, Spain – Part 1: Simulation of diurnal circulation regimes, *Atmos. Chem. Phys.*, 7, 1835–1849, 2007, <http://www.atmos-chem-phys.net/7/1835/2007/>. 10481
- Peters, W., Jacobson, A. R., Sweeney, C., Andrews, A. E., Conway, T. J., Masarie, K., Miller, J. B., Bruhwiler, L. M. P., Pétron, G., Hirsch, A. I., Worthy, D. E. J., van der Werf, G. R., Randerson, J. T., Wennberg, P. O., Krol, M. C., and Tans, P. P.: An atmospheric perspective on North American carbon dioxide exchange: CarbonTracker, *Proc. Natl. Acad. Sci.*, 104, 18925–18930, 2007. 10480
- Sarrat, C., Noilhan, J., Lacarrère, P., Ceschia, E., Ciais, P., Dolman, A. J., Elbers, J. A., Gerbig, C., Gioli, B., Lauvaux, T., Miglietta, F., Neininger, B., Ramonet, M., Vellinga, O., and Bonnefond, J. M.: Mesoscale modelling of the CO₂ interactions between the surface and the atmosphere applied to the April 2007 CERES field experiment, *Biogeosciences*, 6, 633–646, 2009, <http://www.biogeosciences.net/6/633/2009/>. 10486, 10497
- Schmid, H. P.: Footprint modeling for vegetation atmosphere exchange studies: a review and perspective, *Agr. For. Meteorol.*, 113, 159–183, 2002. 10496
- Schmitgen, S., Geiss, H., Ciais, P., Neininger, B., Brunet, Y., Reichstein, M., Kley, D., and Volz-Thomas, A.: Carbon dioxide uptake of a forested region in southwest France derived from airborne CO₂ and CO measurements in a quasi-Lagrangian experiment, *J. Geophys. Res.-Atmos.*, 1–15, 109, 2004. 10481
- Sellers, P. J., Hall, F. G., Asrar, G., Strebel, D. E., and Murphy, R. E.: The first ISLSCP field experiment (FIFE), *B. Am. Meteorol. Soc.*, 69, 22–27, 1988. 10481
- Vaccari, F. P., Gioli, B., Zaldei, A., Sabatini, F., Georgiadis, T., Rossi, F., Peressotti, A., Magliulo, V., and Miglietta, F.: Net Ecosystem Carbon Exchange (NEE) of the Island of Pianosa, *J.*

BGD

6, 10479–10517, 2009

**Regional carbon
fluxes from airborne
flight-path
segmentation**O. S. Vellinga et al.

Title Page

Abstract

Introduction

Conclusions

References

Tables

Figures

◀

▶

◀

▶

Back

Close

Full Screen / Esc

Printer-friendly Version

Interactive Discussion

Mediterra. Ecol., 5, 53–60, 2004. 10481
Vila-Guerau de Arellano, J., Gioli, B., Miglietta, F., Jonker, H. J. J., Baltink, H. K., Hutjes, R. W. A., and Holtslag, A. A. M.: Entrainment process of carbon dioxide in the atmospheric boundary layer, J. Geophys. Res.-Atmos., 109, 1–15, 2004. 10481

BGD

6, 10479–10517, 2009

**Regional carbon
fluxes from airborne
flight-path
segmentation**

O. S. Vellinga et al.

Title Page

Abstract

Introduction

Conclusions

References

Tables

Figures



Back

Close

Full Screen / Esc

Printer-friendly Version

Interactive Discussion

10503



Regional carbon fluxes from airborne flight-path segmentation

O. S. Vellinga et al.

Table 1. Performed measurement flights during IOP 1 (18–22 Apr.) and IOP 2 (7–14 Sep.) at CERES’07 (LA = Lamasquère; MA = Marmande; VI = Villeneuve/s Lot).

Transect	IOP 1		IOP 2
	short	long	long
Segments	3–7	3–12	1–12
Passes	8	10	8
Start Track	VI	VI	MA
End Track	FR	LA	LA
Distance (km)	84	173	218
Time Period (LT)	09:30–11:45	13:45–19:30	09:30–16:45
Height (m agl)	≈ 78	≈ 79	≈ 90
Ground Speed (m/s)	≈ 38	≈ 38	≈ 37

Title Page

Abstract

Introduction

Conclusions

References

Tables

Figures



Back

Close

Full Screen / Esc

Printer-friendly Version

Interactive Discussion

Regional carbon fluxes from airborne flight-path segmentation

O. S. Vellinga et al.

Table 2. Landscape characteristics of segments along flight tracks in the CERES experimental domain (See text for abbreviations).

Segment	Length km	Area km ²	Terrain	Soil Type	Land-Use (fraction 3 km class (%))
1	26	74	river valley	loam	mg (63), ccp/wc (14)
2	30	82	hills NE	clay, loam	ccp/sc (39), pa (17), wm (12)
3	14	28	hills NE	clay, loam	wm (36), ccp/sc (29), pa (12)
4	30	91	hills NE	clay, loam	ccp/wc (45), ccp/sc (16), agr clusters (14), wm (12)
5	15	40	river valley, river	loam	mg (43), ccp/wc (14), fb (13)
6	13	29	river valley	loam	mg (32), fo (22), ccp/sc (15), ccp/wc (14), wm (10)
7	24	70	river valley	loam	vy (49), mg (21), ccp/wc (13)
8	5	14	river valley, river	loam	mg (53), ccp/wc (16), broad leaf + crop (11)
9	24	58	hills SW	loam	mg (42), wm (22), ccp/wc (21)
10	16	35	hills SW	clay	wc (94)
11	20	56	hills SW	clay	wc (87)
12	12	43	river valley	clay, loam	mg (37), ccp/wc (27), wm (25)

Title Page

Abstract

Introduction

Conclusions

References

Tables

Figures



Back

Close

Full Screen / Esc

Printer-friendly Version

Interactive Discussion



Regional carbon fluxes from airborne flight-path segmentation

O. S. Vellinga et al.

Table 3. Segment averages from airborne data along flight tracks during IOP 1 (18–22 Apr.) at CERES’07.

Segment	LAI	fCO_2 $\mu\text{mol}/\text{m}^2/\text{s}$	β	E_f	Q^* W/m^2
1	0.78	n/a	n/a	n/a	n/a
2	1.55	n/a	n/a	n/a	n/a
3	1.73	-10.4	0.63	0.61	563
4	1.36	-7.2	0.59	0.63	547
5	1.20	-4.9	0.53	0.66	553
6	1.66	-0.6	0.77	0.59	574
7	1.26	-3.6	0.36	0.74	543
8	1.26	-4.7	0.32	0.77	522
9	1.42	-6.7	0.48	0.68	504
10	1.42	-11.6	0.45	0.69	487
11	1.56	-13.0	0.38	0.73	505
12	1.50	-6.1	0.60	0.64	489

Title Page

Abstract

Introduction

Conclusions

References

Tables

Figures

⏪

⏩

◀

▶

Back

Close

Full Screen / Esc

Printer-friendly Version

Interactive Discussion

**Regional carbon
fluxes from airborne
flight-path
segmentation**

O. S. Vellinga et al.

Table 4. Same as table 3 except during IOP 2 (7–14 Sep.) at CERES'07.

Segment	LAI	fCO_2 $\mu\text{mol}/\text{m}^2/\text{s}$	β	E_f	Q^* W/m^2
1	1.42	n/a	n/a	n/a	n/a
2	1.10	n/a	n/a	n/a	n/a
3	1.07	n/a	n/a	n/a	n/a
4	0.94	-3.26	1.80	0.36	434
5	1.08	-3.96	1.29	0.44	453
6	1.39	-5.81	1.64	0.39	470
7	0.84	-4.30	1.73	0.38	469
8	0.81	-3.38	2.14	0.33	468
9	0.90	-5.78	1.88	0.36	486
10	0.63	-1.87	2.02	0.34	489
11	0.60	-0.99	2.55	0.31	449
12	0.84	-4.58	2.03	0.35	461

Title Page

Abstract

Introduction

Conclusions

References

Tables

Figures

⏪

⏩

◀

▶

Back

Close

Full Screen / Esc

Printer-friendly Version

Interactive Discussion

Regional carbon fluxes from airborne flight-path segmentation

O. S. Vellinga et al.

Table 5. Average data at ground sites between 1200–1400 UTC (= LT - 2) during IOP 1 (18–22 Apr.) and IOP 2 (7–14 Sep.) at CERES’07.

Station	Vegetation	LAI	$f\text{CO}_2$ $\mu\text{mol}/\text{m}^2/\text{s}$	β	E_f
IOP 1					
Marmande	maize	0	3.3	2.88	0.26
St. Sardos	grass	3.9	-23.2	0.26	0.79
Auradé	sunflower	0	0.3	0.78	0.56
Lamasquère	winter wheat	4.3	-33.6	0.08	0.92
Le Fauga	fallow/grass	n/a	-15.6	0.26	0.79
IOP 2					
Marmande	maize	≈ 4	-20.3	0.84	0.54
St. Sardos	grass	n/a	-1.6	1.68	0.37
Auradé	sunflower	0	0.6	2.91	0.26
Lamasquère	winter wheat	0	-0.2	3.83	0.21
Le Fauga	fallow/grass	n/a	-2.4	4.39	0.19

Title Page

Abstract Introduction

Conclusions References

Tables Figures

⏪ ⏩

◀ ▶

Back Close

Full Screen / Esc

Printer-friendly Version

Interactive Discussion



**Regional carbon
fluxes from airborne
flight-path
segmentation**

O. S. Vellinga et al.

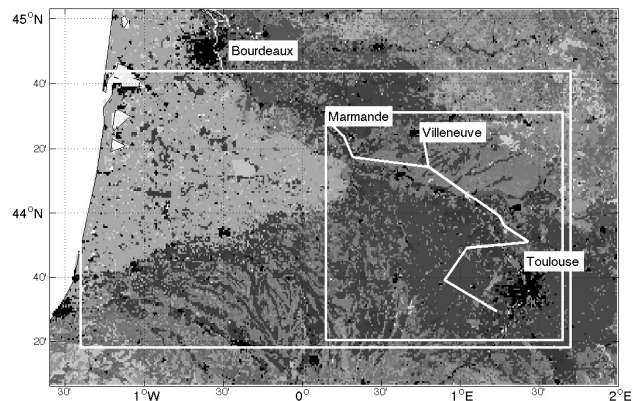


Fig. 1. Enhanced 250-m resolution CORINE 2000 land-use map of southwest France with experimental domain of CERES'07 measurement campaign (outer box) with our flight domain (inner box).

[Title Page](#)[Abstract](#)[Introduction](#)[Conclusions](#)[References](#)[Tables](#)[Figures](#)[⏪](#)[⏩](#)[◀](#)[▶](#)[Back](#)[Close](#)[Full Screen / Esc](#)[Printer-friendly Version](#)[Interactive Discussion](#)

Regional carbon fluxes from airborne flight-path segmentation

O. S. Vellinga et al.

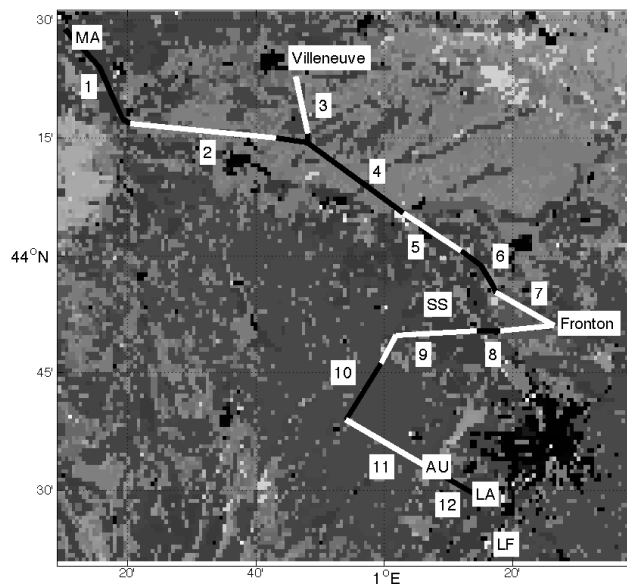


Fig. 2. Inner box from figure 1 with flight tracks divided into 12 segments (B/W) and ground flux sites (2-character labels; see text for abbreviations) in the direct vicinity.

Title Page

Abstract

Introduction

Conclusions

References

Tables

Figures

⏪

⏩

◀

▶

Back

Close

Full Screen / Esc

Printer-friendly Version

Interactive Discussion

Regional carbon fluxes from airborne flight-path segmentation

O. S. Vellinga et al.

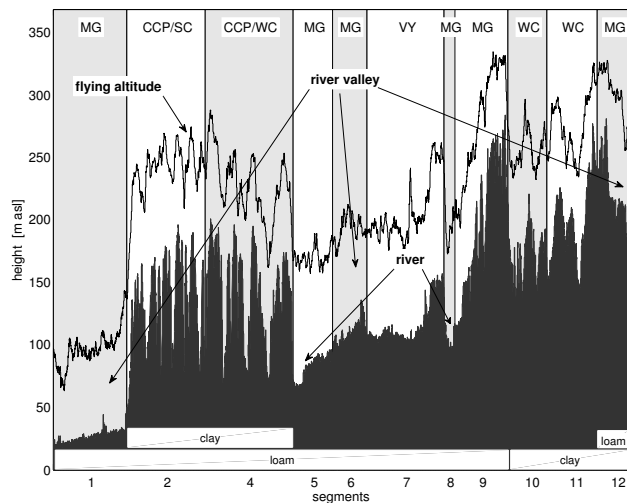


Fig. 3. Terrain elevation along flight track and flying altitude between Marmande to Lamasquère (left to right) at CERES’07, including segments with labels of main land-use classes (2-character labels; see text for abbreviations) and main soil type (bars).

Title Page

Abstract

Introduction

Conclusions

References

Tables

Figures



Back

Close

Full Screen / Esc

Printer-friendly Version

Interactive Discussion

Regional carbon fluxes from airborne flight-path segmentation

O. S. Vellinga et al.

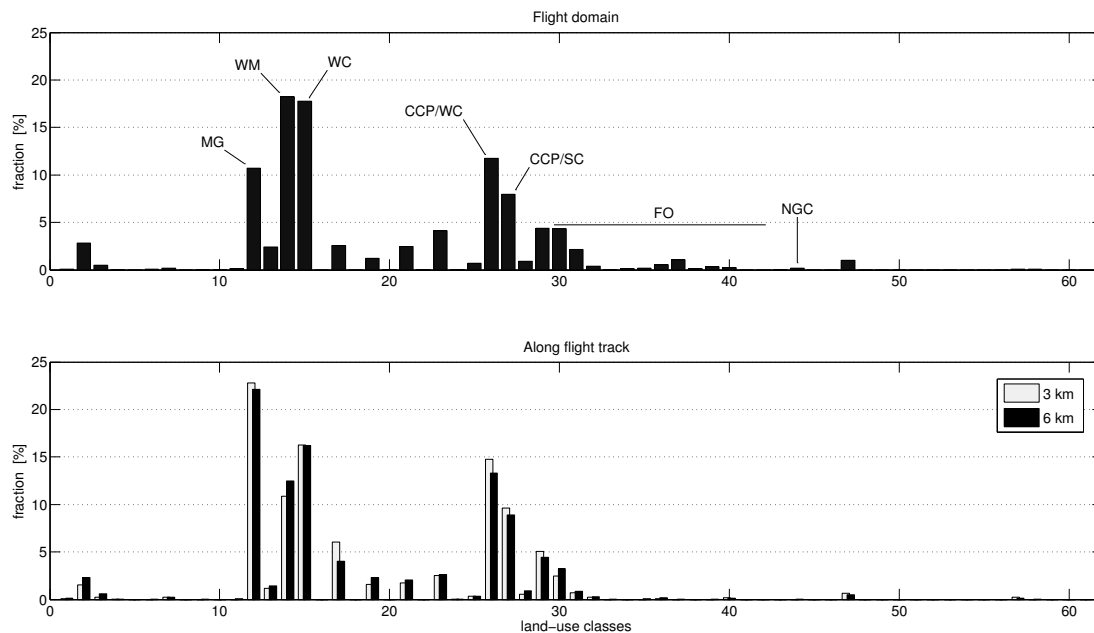


Fig. 4. Histogram of land-use classes for the whole flight domain (upper plot) and along flight track (lower plot) with 3-km and 6-km width at both sides at CERES'07 (See text for abbreviations).

Title Page

Abstract

Introduction

Conclusions

References

Tables

Figures

⏪

⏩

◀

▶

Back

Close

Full Screen / Esc

Printer-friendly Version

Interactive Discussion

Regional carbon fluxes from airborne flight-path segmentation

O. S. Vellinga et al.

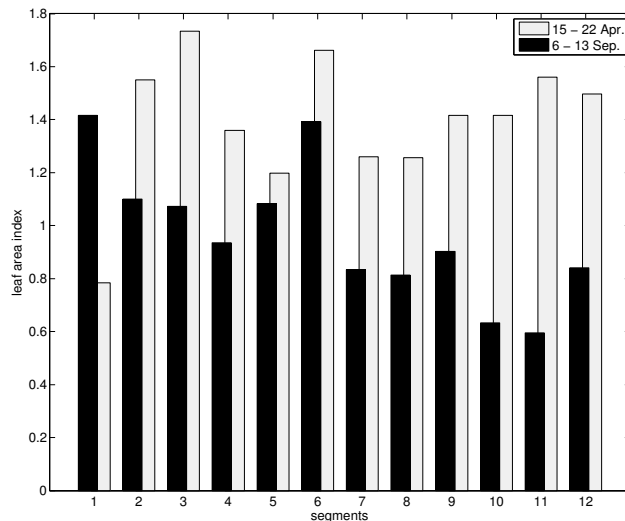


Fig. 5. Average leaf area index per segment along flight track with 3 km width at both sides for 15–22 Apr. and for 6–13 Sep. from MODIS (8-day composite; 250 m resolution).

Title Page

Abstract

Introduction

Conclusions

References

Tables

Figures



Back

Close

Full Screen / Esc

Printer-friendly Version

Interactive Discussion

Regional carbon fluxes from airborne flight-path segmentation

O. S. Vellinga et al.

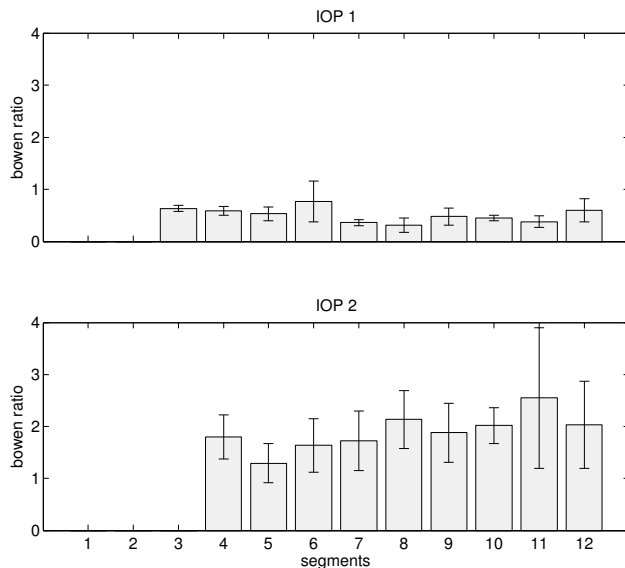


Fig. 6. Average Bowen ratio per segment along flight track during IOP 1 (18–22 Apr.) and IOP 2 (7–14 Sep.) at CERES'07.

Title Page

Abstract

Introduction

Conclusions

References

Tables

Figures

⏪

⏩

◀

▶

Back

Close

Full Screen / Esc

Printer-friendly Version

Interactive Discussion



Regional carbon fluxes from airborne flight-path segmentation

O. S. Vellinga et al.

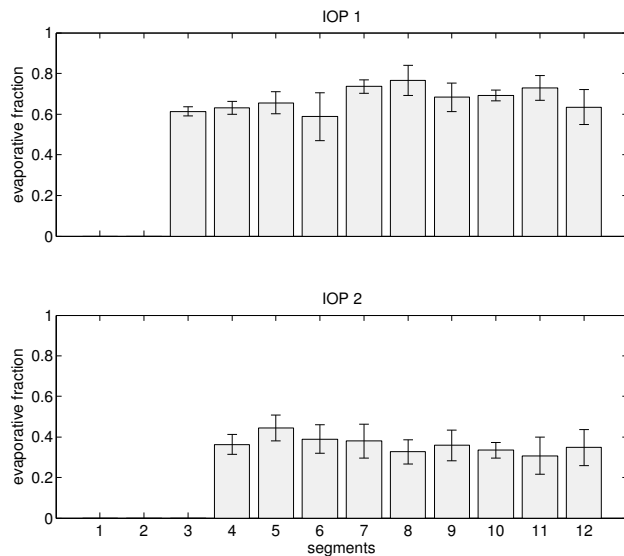


Fig. 7. Average evaporative fraction per segment along flight track during IOP 1 (18–22 Apr.) and IOP 2 (7–14 Sep.) at CERES’07.

Title Page

Abstract

Introduction

Conclusions

References

Tables

Figures

⏪

⏩

◀

▶

Back

Close

Full Screen / Esc

Printer-friendly Version

Interactive Discussion

Regional carbon fluxes from airborne flight-path segmentation

O. S. Vellinga et al.

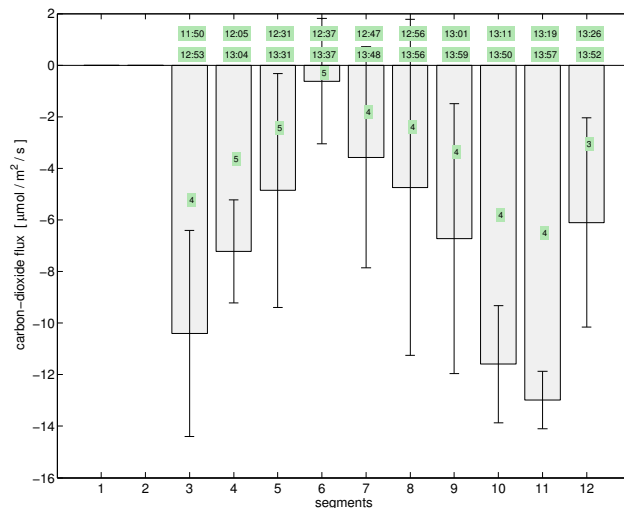


Fig. 8. Average carbon-dioxide flux per segment between 11:50 and 14:00 UTC (= LT -2) along flight track during IOP 1 (18–22 Apr.) at CERES’07, where negative values mean carbon uptake.

Title Page

Abstract

Introduction

Conclusions

References

Tables

Figures

⏪

⏩

◀

▶

Back

Close

Full Screen / Esc

Printer-friendly Version

Interactive Discussion

Regional carbon fluxes from airborne flight-path segmentation

O. S. Vellinga et al.

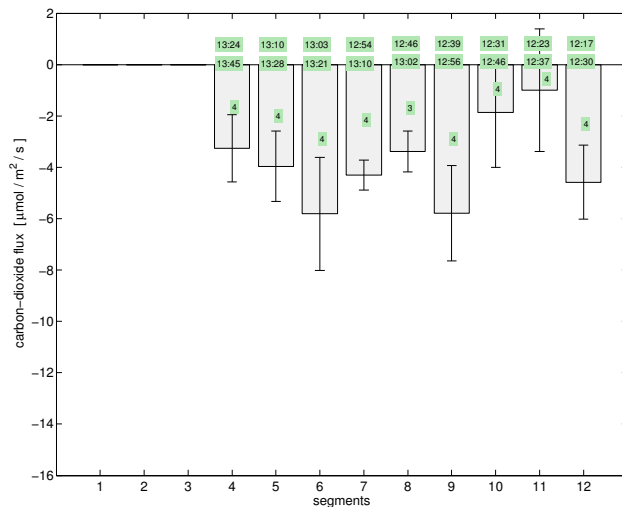


Fig. 9. Same as figure 8 except during IOP 2 (7–14 Sep.) at CERES'07.

Title Page

Abstract

Introduction

Conclusions

References

Tables

Figures

⏪

⏩

◀

▶

Back

Close

Full Screen / Esc

Printer-friendly Version

Interactive Discussion